The Journal of Chemical Physics ARTICLE scitation.org/journal/jcp

Redox states of dinitrogen coordinated to a molybdenum atom

Cite as: J. Chem. Phys. 154, 224308 (2021); doi: 10.1063/5.0050596
Submitted: 16 March 2021 • Accepted: 20 May 2021 •
Published Online: 11 June 2021

Maria V. White, Justin K. Kirkland, and Konstantinos D. Vogiatzis[a]

AFFILIATIONS

Department of Chemistry, University of Tennessee, Knoxville, Tennessee 37996-1600, USA

[a]Author to whom correspondence should be addressed: kvogiatz@utk.edu

ABSTRACT

Chemical structures bearing a molybdenum atom have been suggested for the catalytic reduction of N_2 at ambient conditions. Previous computational studies on gas-phase MoN and MoN_2 species have focused only on neutral structures. Here, an *ab initio* electronic structure study on the redox states of small clusters composed of nitrogen and molybdenum is presented. The complete-active space self-consistent field method and its extension via second-order perturbative complement have been applied on $[MoN]^n$ and $[MoN_2]^n$ species ($n = 0, 1\pm, 2\pm$). Three different coordination modes (end-on, side-on, and linear NMoN) have been considered for the triatomic $[MoN_2]^n$. Our results demonstrate that the reduced states of such systems lead to a greater degree of N_2 activation, which can be the starting point of different reaction channels.

I. INTRODUCTION

The catalytic activation of the N–N bond is an important industrial process for the formation of ammonia, a raw material for the synthesis of fertilizers and other nitrogen-containing molecules and materials, but the dinitrogen functionalization under ambient conditions still remains a challenge due to the thermodynamic stability of the N_2 molecule. The Haber–Bosch process persists to this day as the main industrial procedure for the production of ammonia, a process that requires high pressure and high temperature conditions. On the other hand, biological enzymes can fix nitrogen from the air under ambient conditions. Nitrogenase contains an eight-metal active site, the FeMo-cofactor, where the N_2 bond is reduced and converted into ammonia and other nitrogen compounds. The composition of the active site is known to be Fe_7MoS_9C.[1] While the exact binding site of the substrate is still a topic of active research, the Mo unit potentially plays a role in the activation of dinitrogen. This biological process has inspired interest in the development of synthetic catalysts that could reduce N_2 at ambient conditions. Since the synthesis of the first transition metal complex bound to a dinitrogen ligand,[2] $[Ru(NH_3)_5N_2]^{2+}$, much effort has been expended in the development of coordinated N_2 complexes to assist in the synthesis of ammonia.[3–13]

Molybdenum is one of the most azophilic metals of the *d*-block, and the synthesis and characterization of catalytic Mo-based complexes that can fix N_2 has been the topic of numerous studies.[5,14–17] Moderate ammonia yields have been attained under ambient conditions utilizing complexes bearing molybdenum metal centers, and intriguing reactivities have been shown for Mo complexes under different ligand environments.[18–24] Eizawa *et al.*[22] reported the formation of up to 230 equivalents of ammonia utilizing dimolybdenum complexes bearing phosphine PCP-pincer ligands and *N*-heterocyclic carbenes. In addition, they showed with a detailed density functional theory (DFT) analysis that PCP-pincer ligands serve as σ-donors and π-acceptors, allowing for the strong link between molybdenum and nitrogen atoms. Sita *et al.* developed a chemical cycle using metal mediated complexes composed of molybdenum and tungsten for the production of isocyanates through the activation of dinitrogen.[18] Isocyanates are exemplary synthetic targets because they help us to offset the free energy associated with the breaking of the dinitrogen bond. Using a tridentate phosphine molybdenum system, Liao *et al.* studied the transition-metal-catalyzed formation of silylamine.[19] Furthermore, they showed for the first time that the N–N bond of the hydrazido complex could be split via reduction to form the nitrido complex, with the formation of bissilylamide. The Chatt cycle suffers from the presence of anionic coligands, which cause disproportionation in the first molybdenum stage.[25] New multidentate phosphine ligands have been developed by Hinrichsen *et al.* in order to remedy this problem.[20] Other methods are being examined such as ammonia

synthesis via electrocatalytic nitrogen reduction reaction (NRR). This method appears to be a prominent alternative to the current industrial technology. Finally, the first electrocatalytic NRR under ambient conditions using nitrogen-doped porous carbon with anchored single Mo atoms was recently reported.[23]

In addition to experimental studies, substantial work has been performed on molybdenum-based complexes for N_2 activation on a theoretical level. Smaller systems, such as MoN_x, have been previously analyzed in the gas phase at a theoretical level in order to understand their electronic properties. Computational studies of the neutral states of MoN and MoN_2 have been performed via different levels of theory in order to elucidate the electronic effects that promote the dissociation of the triple bond of N_2 between the constituents.[26–36] An early multireference configuration-interaction (MRCI) study discussed the low-lying states of MoN and highlighted the triple bond between Mo and N.[34] Pyykkö and Tamm performed calculations for the end-on and side-on isomers of MoN_2 in order to elucidate multiple minima on the potential energy surfaces (PESs) of the species under consideration.[31] The authors applied density functional theory (DFT) together with a variety of post-Hartree–Fock methods, and they provided a detailed molecular orbital analysis related to the N_2 binding and activation. Three independent DFT studies focused on the reaction of a neutral Mo with N and N_2 and reported binding energies and harmonic frequencies of different electronic and spin states.[32,33,35]

The aforementioned studies concluded that binding and activation of N_2 on a neutral Mo atom is unfavorable. The energetically most stable isomer of the MoN_2 system has a linear geometry with N_2 weakly bound on Mo through noncovalent interactions, while a side-on isomer with a dissociated N_2 molecule is about 20 kcal/mol less stable. Here, we further expand these studies by examining the electronic structure of ionic states of $[MoN_2]^n$, where $n = 0, \pm1, \pm2$. Our aim is to examine the N_2 activation channels from charged Mo sites by means of multiconfigurational quantum chemical calculations, which elucidate the underlying electronic structure effects of metal–N_2 reactivity. Thus, the analysis and conclusions presented in this work can be used as the basis for future computational and experimental studies that bridge the electronic structure of the bare metal–N_2 clusters with the coordination chemistry of a molecular complex. For example, gas-phase mass spectrometry[37,38] and computational studies[39,40] on the activation of small molecules by mono-ligated metal centers provide vital insights into the reactivity of the more complex counterparts. In addition, the redox states of molybdenum nitride $[MoN]^n$ ($n = 0, \pm1, \pm2$) were also included. All species considered in this study are shown in Fig. 1. Section II presents the computational details of the multiconfigurational methods applied on this study. Our results are presented in Sec. III, and a short discussion is provided in Sec. IV.

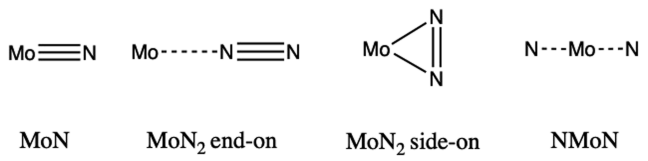

FIG. 1. Coordination modes between nitrogen and molybdenum considered in this study.

II. METHODS

The state-specific and state-average complete active space self-consistent field (CASSCF)[41,42] and its extension through second-order perturbation theory (CASPT2) were employed in this study.[43,44] All calculations were performed with the open-source OpenMolcas program package[45] using the ANO-RCC-VTZP triple-ζ relativistic basis set for all atoms (Mo: 7*s*6*p*4*d*2*f*1*g* and N: 4*s*3*p*2*d*1*f*).[46,47] In all calculations, scalar relativistic effects were included using a second-order Douglas–Kroll–Hess Hamiltonian.[48,49] In the CASPT2 step, an Ionization Potential - Electron Affinity (IPEA) shift of 0.25 and an imaginary shift of 0.20 a.u. were applied.[50,51] All calculations were performed under the C_{2v} point group, including the linear NMoN (C_{2v} was preferred instead of the higher Abelian point group for consistency with respect to the other molecular species). For the linear molecules $[MoN]^n$, $[NMoN]^n$, and end-on $[MoN_2]^n$ ($n = 0, \pm1, \pm2$), the LINEAR keyword of OpenMOLCAS was used.

The CAS(n, m) nomenclature is followed throughout this article for the definition of the selected active space, where n is the number of electrons and m is the number of active orbitals. For the molybdenum nitride species, the valence 2*p* orbitals of the nitrogen and the valence 5*s*4*d* orbitals of the molybdenum were included within the active space, which give rise to a CAS(n,9). The number of electrons n varies based on the total charge of the diatomic molecule. In the case of the MoN_2 end-on, side-on, and linear NMoN species, the three 2*p* orbitals of the additional nitrogen were included for the formation of a CAS(n,12).

The potential energy curves (PECs) of the diatomic Mo–N were constructed by placing the Mo atom at the origin of the Cartesian coordinate system while stretching N along the z-axis for a given set of distances. For the neutral surface, energies were computed from R_{Mo-N} = 1.45 until 10.00 Å with displacement steps of 0.25 Å from 1.45 until 2.175 Å, by 0.1 Å from 2.20 to 5.50 Å, and then at 6.00, 8.00, and 10.00 Å. For the redox cases, energies were computed for R_{Mo-N} = 1.45–4.00 Å by steps of 0.05 Å (1.45 until 2.00 Å) and steps of 1.0 Å (2.00 until 4.00 Å). For the end-on MoN_2 isomer, the potential energy surface (PES) was generated by placing the central N atom at the origin and stretching Mo in the −z direction and the remaining nitrogen in the +z direction. For the neutral species, 0.5 Å displacement points for R_{Mo-N} = 1.00–10.00 Å and 0.05 Å for R_{N-N} = 0.80–1.50 Å were considered and additional points were added closer to the equilibrium distance (R_{Mo-N} = 1.90 –2.50 Å by 0.05 Å and R_{N-N} = 1.10–1.80 Å by 0.01 Å). All redox states of the end-on MoN_2 were computed between the intervals R_{Mo-N} = 1.00–10.00 Å (0.5 Å displacement) and R_{N-N} = 0.80–1.50 Å (0.05 Å displacement). The PES for the side-on MoN_2 isomer was constructed by stretching the dinitrogen molecule along the y-axis and the Mo atom along the z-axis, with R_{Mo-N_2} = 1.00–10.00 Å (0.5 Å displacement) and R_{N-N} = 0.80–3.00 Å (0.1 Å displacement), for both neutral and redox species. Finally, potential energy curves of the linear N–Mo–N complex were computed by the symmetric stretch of the Mo–N bond distances between 0.80 and 5.00 Å (0.05 Å displacement) for both neutral and redox species.

III. RESULTS

A. MoN

The potential energy curve for the dissociation of neutral MoN species was generated using a CAS(9,9) active space. The CASSCF

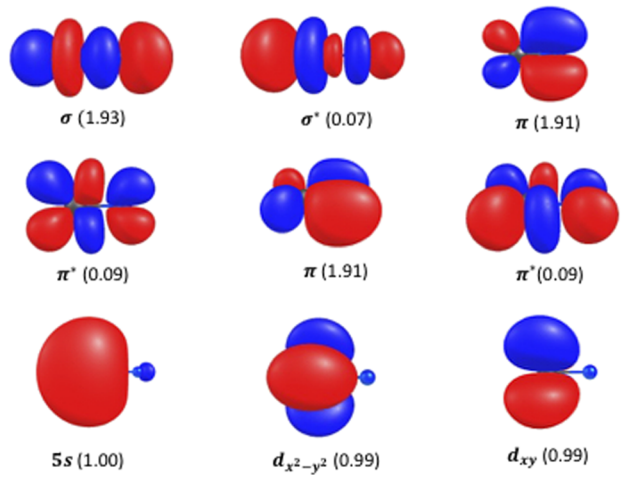

FIG. 2. Natural orbitals and their occupation number (in parentheses) included in the (9,9) active space of the $^4\Sigma^-$ ground state of $[MoN]^0$.

natural orbitals of the ground state of MoN are shown in Fig. 2. These orbitals were obtained at the equilibrium distance (1.645 Å) of the $^4\Sigma^-$ ground state. Different electronic states across a range of spin states were evaluated with CASPT2(9,9). The potential energy curves of the ground state ($^4\Sigma^-$) and the three most stable excited states of $[MoN]^0$ are given in Fig. 3. Excitation energies along with their respective equilibrium internuclear distances, equilibrium bond distances R_{Mo-N}, dissociation energies, and rotational–vibrational constants for the four low-lying states are summarized in Table I. The $^4\Sigma^-$ ground state equilibrium bond distance is at 1.645 Å, in agreement with the experimental value of 1.648 Å[36] and the MRCI value of 1.636 Å of Shim and Gingerich.[34]

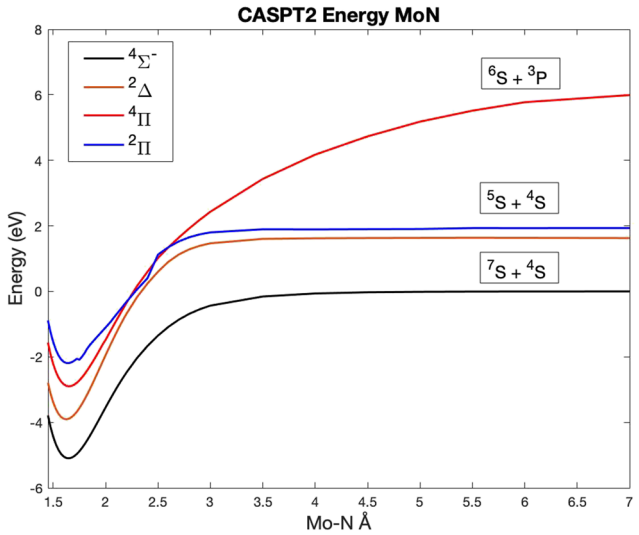

FIG. 3. Potential energy curve of the $^4\Sigma^-$ ground state and the first excited states of $[MoN]^0$ at the CASPT2 level.

TABLE I. Equilibrium bond distances R_{Mo-N} (in Å), dissociation energies D_e and D_0 (in eV), vibrational constants ω_e and $\omega_e\chi_e$ (in cm^{-1}), rotational constants B_e (in cm^{-1}), and excitation energies ΔE (in eV) for the four low-lying states of $[MoN]^0$ obtained at CASPT2(9,9).

State	R_{Mo-N}	D_e	D_0	ω_e	$\omega_e\chi_e$	B_e	ΔE
$^4\Sigma^-$	1.645	5.10	5.03	1031.1	5.3	0.508	0
$^2\Delta$	1.629	5.71	5.65	1084.2	4.0	0.519	1.19
$^4\Pi$	1.651	9.25	9.19	994.6	5.1	0.505	2.19
$^2\Pi$	1.637	4.13	4.06	859.9	−19.2	0.503	2.90

General valance bond (GVB) calculations performed by Allison and Goddard[27] indicated a bond distance of 1.60 Å. We have computed a dissociation energy of 5.10 eV at the CASPT2(9,9) level, which is also in agreement with the experimentally refined value (5.12 eV)[52] and the MRCI value by Stevens *et al.* (5.17 eV).[34] A previous DFT[36] study has analyzed the low-lying states of the MoN diatomic molecule. The authors found that the ground state is $^4\Sigma^-$ and the first excited doublet state $^2\Delta$ is 0.79 eV higher (BP86 functional, QZ4P basis set). Their results are in qualitative agreement with the new results presented in this study. CASPT2(9,9) identified $^4\Sigma^-$ and $^2\Delta$ as the most stable states, but with a relative energy difference of 1.19 eV. Figure 3 also includes the atomic term symbols at the dissociation limit. The ground state dissociates into the ^7S and ^4S terms of the Mo and N atoms, respectively. The Mo atom has the neutral electronic configuration $5s^14d^5$, and the N atom has a $2p^3$ electronic configuration. The doubly degenerate $^2\Delta$ excited state has an excitation energy of 1.19 eV and dissociates into the ^5S and ^4S terms for Mo and N atoms, respectively. A $5s^24d^4$ electronic configuration is observed for Mo where the electron of the $4d_{x^2-y^2}$ atomic orbital is promoted to the 5*s* orbital. The $2p^3$ electronic configuration remains consistent for the N atom. The same dissociation terms are observed for the doubly degenerate $^2\Pi$ excited state with an excitation energy of 2.90 eV. In this case, the electron is promoted to the 5*s* orbital of Mo from the $4d_{yz}$ atomic orbital. Finally, the $^4\Pi$ state with an excitation energy of 2.19 eV dissociates into the ^6S and ^3P terms of the Mo and N atoms, respectively. The electronic configuration of Mo at the dissociation limit pertains to $5s^04d^5$, while the nitrogen atom is reduced and its configuration becomes $2p^4$.

The redox states of molybdenum nitrate $[MoN]^n(n = 1\pm, 2\pm)$ were analyzed by means of multiconfigurational methods. The ground electronic state, the relative energy difference ΔE from the most stable species ($[MoN]^{1-}$, *vide infra*), the equilibrium distance R_{Mo-N}, and spectroscopic constants for each of the five species are given in Table II. The number of electrons in the active space depends on the total charge, while the number of orbitals was kept constant. The dominant electronic configuration for the ground states of each of the five species with different total charge together with their respective active spaces is shown in Fig. 4. The triple bond between Mo and N for the neutral $[MoN]^0$ is clearly shown on the molecular orbital diagram. Three bonding orbitals formed between the three *p* orbitals of the N atom and the d_{z^2}, d_{xz}, and d_{yz} orbitals of the molybdenum are doubly occupied, while the three non-bonding orbitals $5s, 4d_{x^2-y^2}$, and $4d_{xy}$ remain singly occupied. For the $^3\Sigma^-$ ground state of $[MoN]^{1-}$, the singly occupied non-bonding

TABLE II. Equilibrium bond distances R_{Mo-N} (in Å), dissociation energies D_e and D_0 (in eV), vibrational constants ω_e and $\omega_e\chi_e$ (in cm^{-1}), rotational constants B_e (in cm^{-1}), and excitation energies ΔE (in eV) for $[MoN]^n$ ($n = 0, 1\pm, 2\pm$) obtained at CASPT2(9,9).

	State	R_{Mo-N}	D_e	D_0	ω_e	$\omega_e\chi_e$	B_e	ΔE
$[MoN]^{1-}$	$^3\Sigma^-$	1.658	5.66	5.60	1034.4	4.9	0.500	0
$[MoN]^0$	$^4\Sigma^-$	1.645	5.10	5.03	1031.1	5.3	0.508	0.88
$[MoN]^{2-}$	$^4\Pi$	1.660	2.58	2.51	1110.6	10.2	0.500	4.81
$[MoN]^{1+}$	$^3\Sigma^-$	1.613	4.77	4.70	1079.8	5.3	0.529	8.30
$[MoN]^{2+}$	$^2\Delta$	1.606	4.54	4.47	1076.6	5.8	0.534	24.73

5*s* orbital becomes doubly occupied, thereby stabilizing the complex by 0.88 eV with respect to the neutral $[MoN]^0$ diatomic molecule. Similarly, the dissociation energy increases for the anionic species from 5.10 eV (neutral) to 5.64 eV. Further reduction of $[MoN]^{2-}$ yields a doubly degenerate $^4\Pi$ ground state, wherein the additional electrons occupy both the non-bonding d_{xy} and $d_{x^2-y^2}$ orbitals of Mo and one of the π-antibonding orbitals. For the oxidized $[MoN]^{1+}$ and $[MoN]^{2+}$ species, electrons are removed from the non-bonding orbitals, which give rise to $^3\Sigma^-$ and $^2\Delta$ ground states, respectively. The ΔE energies relative to the equilibrium energy of the most stable diatomic molecule ($[MoN]^{1-}$) show that the ionization of $[MoN]^0$ is an energetically favorable process.

B. MoN_2 end-on

Next, we examined the interaction of dinitrogen with molybdenum. The addition of another nitrogen atom expands the active space from CAS(9,9) to CAS(12,12) to accommodate the additional 2*p* orbitals of the second nitrogen. This CAS is used for the end-on, side-on and linear NMoN isomers of the $[MoN_2]^n$ triatomic molecule ($n = 0, 1\pm, 2\pm$). For the end-on isomer, a two-dimensional potential energy surface was constructed by considering the N–N and Mo–N bond stretch. Table III summarizes the CASPT2(12,12) results for the neutral $[MoN_2]^0$, i.e., excitation and dissociation energies, as well as the equilibrium bond distances R_{Mo-N} and R_{N-N}. The discussion is focused on the most stable state per different spin

TABLE III. Excitation and dissociation energies (in eV) and equilibrium bond distances R_{Mo-N} and R_{N-N} (in Å) for the spin states of the end-on $[MoN]^0$ obtained from CASPT2(12,12).

State	Excitation energy	Dissociation energy	R_{Mo-N}	R_{N-N}
$^7\Sigma^+$	0	0.01	4.50	1.10
$^5\Pi$	0.77	0.75	1.90	1.15
$^3\Pi$	1.94	1.92	1.90	1.16
$^1\Pi$	2.37	2.35	1.90	1.14

($S = 0, 1, 2, 3$). These computations revealed that the ground state is $^7\Sigma^+$, which corresponds to zero binding (0.01 eV) between N_2 and molybdenum, in agreement with previous studies.[31] The doubly degenerate quintet state $^5\Pi$ is 0.77 eV higher than the $^7\Sigma^+$ ground state and shows a weak N_2 binding (dissociation energy of 0.75 eV or 17.3 kcal/mol). CASPT2 results reported by Pyykkö and Tamm are also in close agreement with our calculations (excitation and dissociation energies of 21.2 kcal/mol and 0.92 eV, respectively). N_2 is found to be weakly bound to Mo on the quintet state via bonding between the $4d_{xz}$ orbital of Mo and the $2p_x$ antibonding orbital of the center nitrogen displaying a bond length of 1.15 Å between the nitrogen atoms. In addition, a second molecular orbital displays the electron density between the $4d_{xz}$ orbital of the Mo and both of the nitrogen atoms. This molecular orbital is mostly polarized toward the nitrogen atoms. The same kind of electron polarization is observed between the $4d_{yz}$ orbital of the Mo and the nitrogen atoms. The triplet doubly degenerate $^3\Pi$ state was found to be 1.94 eV higher than the septet ground state, which has a strong N_2 binding character (dissociation energy of 1.92 eV). A similar bonding behavior is observed, although π-backbonding was found between the $4d_{yz}$ orbital of the Mo and the central nitrogen atoms.

The results collected for the ionic states of $[MoN_2]^n$ ($n = 1\pm, 2\pm$) are summarized in Table IV. For the 1+ charged species, three states were analyzed utilizing state-average CASSCF and multi-state CASPT2. Excitation energies (ΔE) and dissociation energies (E_{diss}) are shown in Table IV. For the end-on species, the lowest energy state at the dissociation for each given charge was also

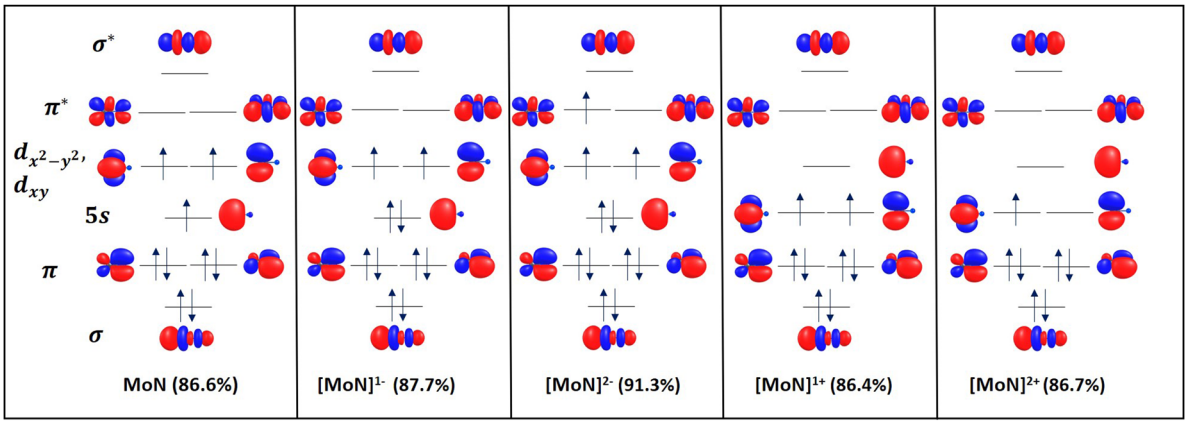

FIG. 4. Molecular orbital diagrams together with the dominant electronic configuration in the neutral and charged $[MoN]^n$ ($n = 0, 1\pm, 2\pm$) diatomic molecules.

TABLE IV. Electronic configurations of the ground state of end-on $[MoN_2]^n$, $n = 0, 1\pm, 2\pm$, percent weight of the dominant configurations, equilibrium bond distances R_{Mo-N} and R_{N-N} (in Å), and energies (in eV) obtained at CASPT2(12,12) relative to the minimum of the lowest energy state (1−). ΔE correspond to relaxed energies.

	State	Active space	Configuration	% weight	ΔE	E_{diss}	R_{Mo-N}	R_{N-N}
$[MoN_2]^{1-}$	$^6\Sigma^+$	(13,12)	$(\sigma)^2(\pi)^4(2s)^2(d_{xz})^1(d_{yz})^1(d_{xy})^1(d_{z^2})^1(d_{x^2-y^2})^1(\sigma^*)^0(\pi^*)^0$	93.1	0	0	-	1.10
$[MoN_2]^0$	$^7\Sigma^+$	(12,12)	$(\sigma)^2(\pi)^4(5s)^1(d_{xz})^1(d_{yz})^1(d_{xy})^1(d_{z^2})^1(d_{x^2-y^2})^1(\sigma^*)^0(\pi^*)^0$	93.5	0.31	0.01	4.50	1.10
$[MoN_2]^{2-}$	$^5\Pi$	(14,12)	$(\sigma)^2(\pi)^4(2s)^2(d_{xz})^1(d_{yz})^1(d_{xy})^1(d_{z^2})^1(d_{x^2-y^2})^1(\sigma^*)^1(\pi^*)^0$	53.2	3.87	0.58	10.0	1.20
$[MoN_2]^{1+}$	$^6\Sigma^+$	(11,12)	$(\sigma)^2(\pi)^4(d_{xz})^1(d_{yz})^1(d_{xy})^1(d_{z^2})^1(d_{x^2-y^2})^1(5s)^0(\sigma^*)^0(\pi^*)^0$	93.3	6.88	0.59	2.50	1.10
$[MoN_2]^{2+}$	$^5\Sigma^+$	(10,12)	$(\sigma)^2(\pi)^4(d_{xz})^1(d_{yz})^1(d_{xy})^1(d_{x^2-y^2})^1(5s)^0(d_{z^2})^0(\sigma^*)^0(\pi^*)^0$	93.1	21.68	1.95	2.00	1.10

the ground state species. No bonding is observed in the charged species. Although the sextet (1−) is lowered in energy than the neutral septet, no binding was observed between Mo and N_2. The electronic configuration of the anionic states shows doubly occupancy for the 2*s* orbital of the nitrogen. We believe that this orbital was introduced into our active space due to radial correlation. The 2− complex displays a N–N bond length of 1.2 Å. This is due to the occupancy of one of the antibonding orbitals of the nitrogen as displayed in the electronic configuration. On the contrary, the oxidized $[MoN_2]^{1+}$ and $[MoN_2]^{2+}$ have a binding character, but they are 6.88 and 21.68 eV less stable than the $[MoN_2]^{1-}$ species, respectively.

C. MoN_2 side-on

The side-on $[MoN_2]^n$ isomer ($n = 0, 1\pm, 2\pm$) was examined by means of multiconfigurational methods. A CAS(12,12) was used for all CASPT2 calculations (see Fig. 5). Table V includes the most stable electronic states per spin multiplicity as well as the excitation and dissociation energies E_{diss}. In addition, the distance at the minimum geometry between Mo–N and N–N is also shown. For the neutral species, the $^7A_1$ state was determined as the ground state geometry where no overlap is found between Mo and N_2. The CASPT2 potential energy surface of the first excited state, $^5B_2$, is shown in Fig. 6. The $^5B_2$ state is only 0.62 eV higher than the septet ground state (Table V). The internuclear distance of the Mo and nitrogen atoms is 2.09 Å, and the bond distance of the dinitrogen is 1.2 Å. This indicates activation of the N_2 bond due to the elongated bond, in agreement with the CASPT2 study of Pyykkö and Tamm. On the contrary, a previous DFT study[32] reported a reverse order for these two states, but the authors commented that this could be due to overbinding of weakly bound systems predicted by standard DFT functionals. Although our geometries for the singlet state agree with the DFT work, again the relative order is reversed. CASPT2(12,12) estimates that the $^1A_1$ neutral state is more stable than the triplet $^3B_2$ by 0.12 eV.

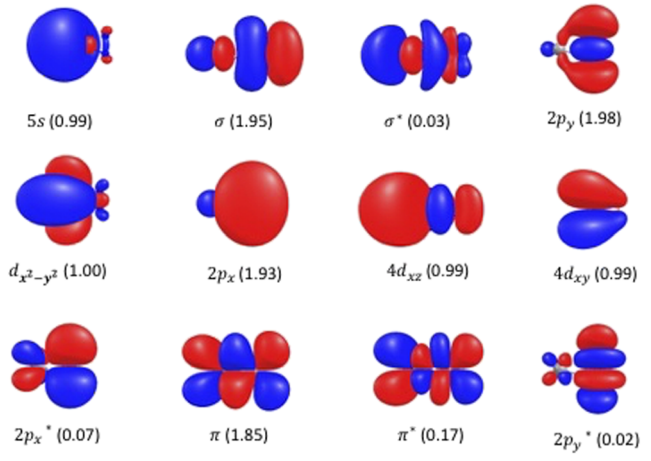

FIG. 5. Natural orbitals and their occupation number (in parentheses) included in the (12,12) active space of the $^5B_2$ state of the side-on $[MoN]^0$.

We now turn our attention to the ionic states of the side-on $[MoN_2]^n$ ($n = 1\pm, 2\pm$). Table VI includes the relative energy differences ΔE with respect to the most stable species of the side-on $[MoN_2]^{1-}$ molecule, which was found again to be more stable than their neutral equivalent. The dominant electronic configuration for the ground states of each of the five species with different total charge together with their respective active spaces is also displayed on Table VI. Dinitrogen is reduced in the case of 1− as seen from its $^2A_1$ ground state, while molybdenum is in oxidation state V. We report this electronic configuration as "Mo(V) + $(N^{-3})_2$." The dissociated dinitrogen bond exhibits a R_{N-N} distance of 2.80 Å (Fig. 7). Reduction of the neutral species lowers the energy by 0.83 eV. Molybdenum is found in the Mo(IV) oxidation state upon further reduction ($[MoN_2]^{2-}$), but this complex is 3.23 eV less stable than the most stable $[MoN_2]^{1-}$ case. Dissociation energies display the same pattern as for the end-on species, increasing in energy from 0.02 (neutral) to 0.55 eV (1−) and to 1.82 eV for the 2− electron reduced species. For the two oxidized species $[MoN_2]^{1+}$ and $[MoN_2]^{2+}$, electrons are removed from the 5*s* and d_{z^2} non-bonding orbitals, yielding $^6A_1$ and $^5A_1$ ground states, respectively. The ΔE energies relative to the most stable side-on species $[MoN_2]^{1-}$ also show that the ionization of $[MoN_2]^0$ is an energetically intense process.

TABLE V. Excitation and dissociation energies (in eV) and equilibrium bond distances R_{Mo-N} and R_{N-N} (in Å) for the spin states of the side-on $[MoN]^0$ obtained from CASPT2(12,12).

State	Excitation energy	E_{diss}	R_{Mo-N}	R_{N-N}
$^7A_1$	0	0.02	4.53	1.10
$^5B_2$	0.62	0.60	2.09	1.20
$^1A_1$	0.85	0.83	1.68	2.70
$^3B_2$	0.97	0.95	1.72	2.80

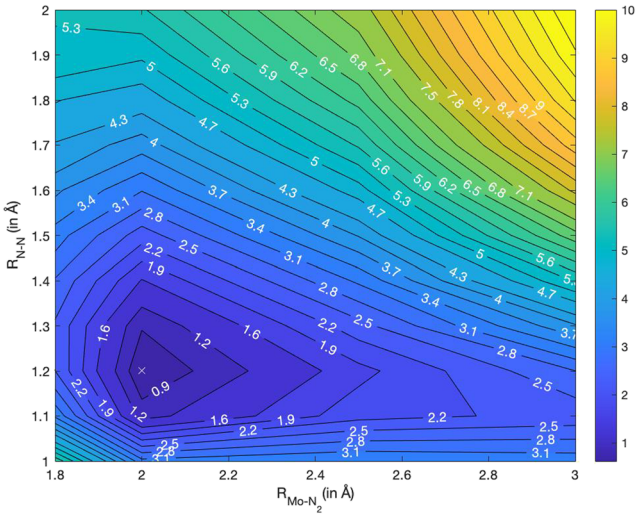

FIG. 6. Relative CASPT2(12,12) energies (in eV) of the $^5B_2$ state of the side-on $[MoN]^0$ species. The X mark indicates the minimum of the potential energy surface.

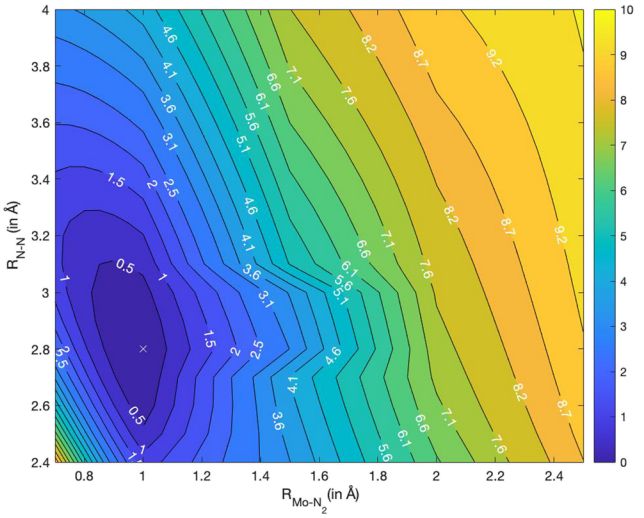

FIG. 7. CASPT2(12,12) potential energy surface (in eV) of the $^2A_1$ state of the side-on $[MoN]^{1-}$. The X mark indicates the minimum of the potential energy surface.

D. Linear NMoN

For the sake of completeness, the linear isomer $[NMoN]^n$, $n = 0, 1\pm, 2\pm$, was examined. In this case, the molybdenum atom is inserted into the dinitrogen molecule and forms a high-energy isomer. All energies, potential energy curves, spectroscopic data, electronic configurations, and molecular orbitals of the CAS(12,12) are presented in detail in the supplementary material. The central molybdenum atom forms two sets of bonding, antibonding, and non-bonding molecular orbitals, $\sigma, \sigma^*, n_\sigma$ and π, π^*, n_π, respectively. For the neutral $[NMoN]^0$ species, the $^3\Sigma_g^-$ ground state has a $(\sigma)^2(\pi)^4(d_{x^2-y^2})^1(d_{xy})^1(n_\pi)^4(5s)^0(n_\sigma)^0(\pi^*)^0(\sigma^*)^0$ dominant configuration. The lowest quintet ($^5\Pi_u$), singlet ($^1\Delta_g$), and septet ($^7\Sigma_u^-$) states are 0.52, 0.71, and 0.93 eV less stable than the ground state. The minimum for all spin states varies in the range of $R_{Mo-N} = 1.70–1.85$ Å, with $R_{Mo-N} = 1.70$ Å for the triplet $^3\Sigma_u^-$ ground state.

We turn now our attention to the redox states. Similar to the end-on and side-on species, the anionic $[NMoN]^{1-}$ was found to be more stable than the neutral $[NMoN]^0$ counterpart by 2.14 eV. The quartet $^4\Sigma_g^-$ spin state is the ground state for the $[NMoN]^{1-}$ case, where the additional electron occupies the 5*s* atomic orbital of molybdenum. The doubly anionic state $^5\Sigma_u^-$ lies 4.15 eV higher than the $^4\Sigma_u^-$ state, while the cationic $^2\Sigma_u^-$ and $^3\Delta_u$ states of $[NMoN]^{1+}$ and $[NMoN]^{2+}$ species, respectively, are more than 10 eV higher than $^4\Sigma_g^-$ (11.32 and 27.35 eV, respectively).

IV. DISCUSSION

The interaction between neutral and ionic states of molybdenum and dinitrogen was investigated. Three different binding modes were considered, the end-on and side-on modes of MoN_2 and a fully dissociated dinitrogen that forms the linear NMoN, and all results are summarized in Table VII. For all charges included in this study, the linear NMoN complex is less stable than the other two isomers, with relative energies that range from 2.23 until 6.38 eV. For that reason, it will be excluded for the rest of the discussion. The $^2A_1$ state of the anionic side-on $[MoN_2]^{1-}$ isomer was found to be the lowest state among all isomers, charges, and spin states considered in this study. The other two anionic isomers with a 1− charge (end-on $[MoN_2]^{1-}$ and linear $[NMoN]^{1-}$) are less stable by 0.53 and 2.23 eV, respectively. Since the minimum of the $^2A_1$ state involves an

TABLE VI. Electronic configurations of the ground state of side-on $[MoN_2]^n$, $n = 0, 1\pm, 2\pm$, percent weight of the dominant configurations, equilibrium bond distances R_{Mo-N} and R_{N-N} (in Å), and energies obtained at CASPT2(12,12) relative to the minimum of the lowest energy state (1−). ΔE correspond to relaxed energies.

	State	Active space	Configuration	% weight	ΔE	E_{diss}	R_{Mo-N}	R_{N-N}
$[MoN_2]^{1-}$	$^2A_1$	(13,12)	$Mo(V) + (N^{-3})_2$	79.3	0	0.55	1.72	2.80
$[MoN_2]^0$	$^7A_1$	(12,12)	$(\sigma)^2(\pi)^4(5\,s)^1(d_{xz})^1(d_{yz})^1(d_{xy})^1(d_{z^2})^1(d_{x^2-y^2})^1(\sigma^*)^0(\pi^*)^0$	93.5	0.83	0.02	4.53	1.10
$[MoN_2]^{2-}$	$^1A_1$	(14,12)	$Mo(IV) + (N^{-3})_2$	74.0	3.23	1.82	1.72	2.80
$[MoN_2]^{1+}$	$^6A_1$	(11,12)	$(\sigma)^2(\pi)^4(d_{xz})^1(d_{yz})^1(d_{xy})^1(d_{z^2})^1(d_{x^2-y^2})^1(5\,s)^0(\sigma^*)^0(\pi^*)^0$	93.5	7.83	0.17	2.56	1.10
$[MoN_2]^{2+}$	$^5A_1$	(10,12)	$(\sigma)^2(\pi)^4(d_{xz})^1(d_{yz})^1(d_{xy})^1(d_{x^2-y^2})^1(5s)^0(d_{z^2})^0(\sigma^*)^0(\pi^*)^0$	93.4	23.19	0.77	2.56	1.10

TABLE VII. Relative energy differences between the end-on MoN_2, side-on MoN_2, and NMoN species, for the neutral and redox states, computed at CASPT2(12,12). The relative energy differences from the ground state of the side-on $[MoN_2]^{1-}$ are shown in parentheses.

	MoN_2 side-on			MoN_2 end-on			NMoN		
Charge	State	ΔE		State	ΔE		State	ΔE	
0	$^7A_1$	0	(0.83)	$^7\Sigma^+$	0	(0.83)	$^3\Sigma_g^-$	3.54	(4.37)
1−	$^2A_1$	0	(0)	$^6\Sigma^+$	0.53	(0.53)	$^4\Sigma_g^-$	2.23	(2.23)
2−	$^1A_1$	0	(3.23)	$^5\Pi$	1.16	(4.40)	$^5\Sigma_u^-$	3.14	(6.38)
1+	$^6A_1$	0	(7.83)	$^6\Sigma^+$	−0.42	(7.41)	$^2\Sigma_u^-$	5.71	(13.54)
2+	$^5A_1$	0	(23.19)	$^5\Sigma^+$	−0.99	(22.20)	$^4\Delta_u$	6.38	(29.57)

activated dinitrogen with R_{N-N} = 2.80 Å, we believe that the reduced species can lead to a dissociation channel relevant to N_2 functionalization. On the contrary, no N_2 activation was observed for the anionic sextet state $^6\Sigma^+$ of the end-on isomer. Upon further reduction ($[MoN_2]^{2-}$), N_2 activation was observed for both coordination modes. The $^5\Pi$ and $^1A_1$ states were determined as the most stable states for the end-on and side-on isomers, respectively, with the $^1A_1$ state being more energetically favorable by 1.16 eV. The singlet state displayed the same geometry as the doublet state of $[MoN_2]^{1-}$, while the $^5\Pi$ state displayed a further elongation of the N_2 bond due to the additional electron occupancy of the antibonding orbital of the dinitrogen.

The two neutral septet states $^7A_1$ and $^7\Sigma^+$ of the side-on and end-on $[MoN_2]^0$, respectively, were found to be 0.83 eV less stable than the global minimum. The CASPT2(12,12) results indicate that these two species are isoenergetic with a relative energy difference of less than 0.1 eV (0.0035 eV). Therefore, the two isomers have similar stabilities since the energy difference falls within the error of the CASPT2 method, a result that suggests a polytopic van der Waals interaction.[53,54] The relative energy difference between the $^7\Sigma^+$ state of the end-on and the most stable end-on MoN_2 isomer with an activated dinitrogen molecule ($^5\Pi$ of end-on, Table III) is 0.77 eV, in agreement with the result reported by Pyykkö and Tamm (0.92 eV).[31]

We have also considered the energetically less favorable isomers for the 1+ and 2+ oxidation states. The relative energy differences displayed in the results allowed us to conclude that such states could be attained only under the presence of a ligand field around a Mo(I) or Mo(II) center. We are currently examining the Mo ligand field effects on the N_2 activation and fixation, which will be the topic of a separate study. For the cationic species, the end-on species were more stable than the side-on isomer by 0.42 and 0.99 eV for the 1+ and 2+ cases, respectively. This conclusion is in contrast to the anionic cases, where the side-on isomer was always more stable than the side-on equivalent. Their electronic configurations of the $^6A_1$ (side-on) and $^6\Sigma^+$ (end-on) were identical, where Mo(I) has five singly occupied 4*d* atomic orbitals and an unoccupied 5*s* orbital. The Mo–N bond distance differed by 0.06 Å between the end-on and side-on isomers, while the N–N remained at its natural bond length. Since the electronic configurations and the bond lengths were found to be nearly identical, the high energy difference can be associated with the ability of Mo to bind easily to one nitrogen rather than to two nitrogen atoms in the angled position. Finally, the quintet spin states were found to be the most stable states for both modes of the 2+ charged species, with a relative energy difference of 0.99 eV. The end-on isomer displayed lower energy at a Mo–N bond distance of 2.00 Å. The Mo–N distance of the side-on isomer was 2.56 Å. Both states displayed a loss of electron density from the 5*s* and $4d_{z^2}$ orbitals of the molybdenum with respect to the neutral species.

V. CONCLUSIONS

A multiconfigurational electronic structure study was performed on different coordination modes of Mo to N and N_2. These species were studied in their neutral and redox states, and we found that the reduced states lead to N_2 activation. The results presented in this study can provide a computational first approach for the understanding of N_2 activation channels when ligand effects of the transition metal are introduced, from mono-ligated to fully coordinated Mo in molecular complexes. Such studies are currently underway in our research group.

SUPPLEMENTARY MATERIAL

See the supplementary material for electronic energies and relative energy differences for all electronic states considered in this study. In addition, it contains rotational–vibrational constants for the most stable states for all molecular systems and a detailed analysis on the NMoN triatomic molecule.

ACKNOWLEDGMENTS

We gratefully acknowledge the National Science Foundation (Grant No. CHE-1800237) for the financial support of this work and the Advanced Computer Facility (ACF) of the University of Tennessee for computational resources.

DATA AVAILABILITY

The data that support the findings of this study are available within the article and its supplementary material.

REFERENCES

[1] K. M. Lancaster, M. Roemelt, P. Ettenhuber, Y. Hu, M. W. Ribbe, F. Neese, U. Bergmann, and S. DeBeer, Science **334**, 974 (2011).
[2] C. V. Senoff, J. Chem. Educ. **67**, 368 (1990).
[3] M. Hidai and Y. Mizobe, Chem. Rev. **95**, 1115 (1995).
[4] M. D. Fryzuk and S. A. Johnson, Coord. Chem. Rev. **200-202**, 379 (2000).
[5] B. A. MacKay and M. D. Fryzuk, Chem. Rev. **104**, 385 (2004).
[6] *Comprehensive Coordination Chemistry II*, edited by J. A. McCleverty and T. J. Meyer (Elsevier, 2004).
[7] M. Hidai and Y. Mizobe, Can. J. Chem. **83**, 358 (2005).
[8] Y. Tanabe and Y. Nishibayashi, Coord. Chem. Rev. **257**, 2551 (2013).
[9] K. C. MacLeod and P. L. Holland, Nat. Chem. **5**, 559–565 (2013).
[10] B. M. Hoffman, D. Lukoyanov, Z.-Y. Yang, D. R. Dean, and L. C. Seefeldt, Chem. Rev. **114**, 4041 (2014).
[11] Y. Nishibayashi, Inorg. Chem. **54**, 9234 (2015).
[12] Y. Tanabe and Y. Nishibayashi, Chem. Rec. **16**, 1549 (2016).
[13] Y. Nishibayashi, Dalton Trans. **47**, 11290 (2018).
[14] K. Shiina, J. Am. Chem. Soc. **94**, 9266 (1972).
[15] J. Chatt, A. J. Pearman, and R. L. Richards, Nature **253**, 39 (1975).
[16] J. Chatt, A. J. Pearman, and R. L. Richards, J. Chem. Soc., Dalton Trans. **1977**, 1852.

[17]D. V. Yandulov and R. R. Schrock, Science **301**, 76 (2003).
[18]A. J. Keane, W. S. Farrell, B. L. Yonke, P. Y. Zavalij, and L. R. Sita, Angew. Chem., Int. Ed. **54**, 10220–10224 (2015).
[19]Q. Liao, N. Saffon-Merceron, and N. Mézailles, ACS Catal. **5**, 6902 (2015).
[20]S. Hinrichsen, A. Kindjajev, S. Adomeit, J. Krahmer, C. Näther, and F. Tuczek, Inorg. Chem. **55**, 8712 (2016).
[21]L. M. Duman and L. R. Sita, J. Am. Chem. Soc. **139**, 17241 (2017).
[22]A. Eizawa, K. Arashiba, H. Tanaka, S. Kuriyama, Y. Matsuo, K. Nakajima, K. Yoshizawa, and Y. Nishibayashi, Nat. Commun. **8**, 14874 (2017).
[23]L. Han, X. Liu, J. Chen, R. Lin, H. Liu, F. Lu, S. Bak, Z. Liang, S. Zhao, E. Stavitski, J. Luo, R. R. Adzic, and H. Xin, Angew. Chem., Int. Ed. **58**, 2321 (2018).
[24]Y. Ashida, K. Arashiba, K. Nakajima, and Y. Nishibayashi, Nature **568**, 536 (2019).
[25]G. C. Stephan, C. Sivasankar, F. Studt, and F. Tuczek, Chem.- Eur. J. **14**, 644 (2008).
[26]J. K. Bates and D. M. Gruen, J. Mol. Spectrosc. **78**, 284 (1979).
[27]J. N. Allison and W. A. Goddard, Chem. Phys. **81**, 263 (1983).
[28]R. C. Carlson, J. K. Bates, and T. M. Dunn, J. Mol. Spectrosc. **110**, 215 (1985).
[29]D. A. Fletcher, K. Y. Jung, and T. C. Steimle, J. Chem. Phys. **99**, 901 (1993).
[30]K. Y. Jung, D. A. Fletcher, and T. C. Steimle, J. Mol. Spectrosc. **165**, 448 (1994).
[31]P. Pyykkö and T. Tamm, J. Phys. Chem. A **101**, 8107 (1997).
[32]A. Martínez, A. M. Köster, and D. R. Salahub, J. Phys. Chem. A **101**, 1532 (1997).
[33]A. Bérces, S. A. Mitchell, and M. Z. Zgierski, J. Phys. Chem. A **102**, 6340 (1998).
[34]I. Shim and K. A. Gingerich, J. Mol. Struct.: THEOCHEM **460**, 123 (1999).
[35]K. L. Brown and N. Kaltsoyannis, J. Chem. Soc., Dalton Trans. **1999**, 4425.
[36]F. Stevens, I. Carmichael, F. Callens, and M. Waroquier, J. Phys. Chem. A **110**, 4846 (2006).
[37]D. Schröder and H. Schwarz, Proc. Natl. Acad. Sci. U. S. A. **105**, 18114 (2008).
[38]V. Blagojevic, V. V. Lavrov, G. K. Koyanagi, and D. K. Bohme, J. Am. Soc. Mass Spectrom. **30**, 1850 (2019).
[39]J. K. Kirkland, S. N. Khan, B. Casale, E. Miliordos, and K. D. Vogiatzis, Phys. Chem. Chem. Phys. **20**, 28786 (2018).
[40]S. N. Khan and E. Miliordos, J. Phys. Chem. A **123**, 5590 (2019).
[41]B. O. Roos, P. R. Taylor, and P. E. M. Siegbahn, Chem. Phys. **48**, 157 (1980).
[42]J. Olsen, B. O. Roos, P. Jørgensen, and H. J. A. Jensen, J. Chem. Phys. **89**, 2185 (1988).
[43]K. Andersson, P. Å. Malmqvist, B. O. Roos, A. J. Sadlej, and K. Wolinski, J. Phys. Chem. **94**, 5483 (1990).
[44]K. Andersson, P. Å. Malmqvist, and B. O. Roos, J. Chem. Phys. **96**, 1218 (1992).
[45]I. F. Galván, M. Vacher, A. Alavi, C. Angeli, F. Aquilante, J. Autschbach, J. J. Bao, S. I. Bokarev, N. A. Bogdanov, R. K. Carlson, L. F. Chibotaru, J. Creutzberg, N. Dattani, M. G. Delcey, S. S. Dong, A. Dreuw, L. Freitag, L. M. Frutos, L. Gagliardi, F. Gendron, A. Giussani, L. González, G. Grell, M. Guo, C. E. Hoyer, M. Johansson, S. Keller, S. Knecht, G. Kovačeviă, E. Källman, G. Li Manni, M. Lundberg, Y. Ma, S. Mai, J. P. Malhado, P. Å. Malmqvist, P. Marquetand, S. A. Mewes, J. Norell, M. Olivucci, M. Oppel, Q. M. Phung, K. Pierloot, F. Plasser, M. Reiher, A. M. Sand, I. Schapiro, P. Sharma, C. J. Stein, L. K. Sørensen, D. G. Truhlar, M. Ugandi, L. Ungur, A. Valentini, S. Vancoillie, V. Veryazov, O. Weser, T. A. Wesołowski, P. O. Widmark, S. Wouters, A. Zech, J. P. Zobel, and R. Lindh, J. Chem. Theory Comput. **15**, 5925 (2019).
[46]B. O. Roos, R. Lindh, P.-Å. Malmqvist, V. Veryazov, and P.-O. Widmark, J. Phys. Chem. A **108**, 2851 (2004).
[47]B. O. Roos, R. Lindh, P.-Å. Malmqvist, V. Veryazov, and P.-O. Widmark, J. Phys. Chem. A **109**, 6575 (2005).
[48]M. Douglas and N. M. Kroll, Ann. Phys. **82**, 89 (1974).
[49]B. A. Hess, Phys. Rev. A **33**, 3742 (1986).
[50]N. Forsberg and P.-Å. Malmqvist, Chem. Phys. Lett. **274**, 196 (1997).
[51]G. Ghigo, B. O. Roos, and P.-Å. Malmqvist, Chem. Phys. Lett. **396**, 142 (2004).
[52]K. A. Gingerich, J. Chem. Phys. **49**, 19 (1968).
[53]E. Clementi, H. Kistenmacher, and H. Popkie, J. Chem. Phys. **58**, 2460 (1973).
[54]A. Papakondylis and A. Mavridis, J. Phys. Chem. A **105**, 7106 (2001).